Experimental High-Frequency Irreversible Electroporation Using a Single-Needle Delivery Approach for Nonthermal Pancreatic Ablation In Vivo

Timothy J. O'Brien, Michael Passeri, Melvin F. Lorenzo, Jesse K. Sulzer, William B. Lyman, Jacob H. Swet, Dionisios Vrochides, Erin H. Baker, David A. Iannitti, Rafael V. Davalos, and Iain H. McKillop

ABSTRACT

Purpose: To investigate the feasibility of single-needle high-frequency irreversible electroporation (SN-HFIRE) to create reproducible tissue ablations in an *in vivo* pancreatic swine model.

Materials and Methods: SN-HFIRE was performed in swine pancreas *in vivo* in the absence of intraoperative paralytics or cardiac synchronization using 3 different voltage waveforms (1-5-1, 2-5-2, and 5-5-5 [on-off-on times (μs)], n = 6/setting) with a total energized time of 100 μs per burst. At necropsy, ablation size/shape was determined. Immunohistochemistry was performed to quantify apoptosis using an anticleaved caspase-3 antibody. A numerical model was developed to determine lethal thresholds for each waveform in pancreas.

Results: Mean tissue ablation time was 5.0 ± 0.2 minutes, and no cardiac abnormalities or muscle twitch was detected. Mean ablation area significantly increased with increasing pulse width (41.0 ± 5.1 mm^2 [range 32–66 mm^2] vs 44 ± 2.1 mm^2 [range 38–56 mm^2] vs 85.0 ± 7.0 mm^2 [range 63–155 mm^2]; 1-5-1, 2-5-2, 5-5-5, respectively; $p < 0.0002$ 5-5-5 vs 1-5-1 and 2-5-2). The majority of the ablation zone did not stain positive for cleaved caspase-3 (6.1 ± 2.8% [range 1.8–9.1%], 8.8 ± 1.3% [range 5.5–14.0%], and 11.0 ± 1.4% [range 7.1–14.2%] cleaved caspase-3 positive 1-5-1, 2-5-2, 5-5-5, respectively), with significantly more positive staining at the 5-5-5 pulse setting compared with 1-5-1 ($p < 0.03$). Numerical modeling determined a lethal threshold of 1114 ± 123 V/cm (1-5-1 waveform), 1039 ± 103 V/cm (2-5-2 waveform), and 693 ± 81 V/cm (5-5-5 waveform).

Conclusions: SN-HFIRE induces rapid, predictable ablations in pancreatic tissue *in vivo* without the need for intraoperative paralytics or cardiac synchronization.

ABBREVIATIONS

HFIRE = high-frequency irreversible electroporation, IHC = immunohistochemistry, IRE = irreversible electroporation, PDAC = pancreatic ductal adenocarcinoma, SN-HFIRE = single-needle high-frequency irreversible electroporation, TTC = triphenyltetrazolium chloride

Pancreatic ductal adenocarcinoma (PDAC) is the third most common cause of cancer-related death in the United States (1,2). Surgical resection offers the best chance for cure, but advanced disease stage at diagnosis means the majority of PDAC patients are not suitable candidates for resection (3). Systemic chemotherapy offers the potential to improve the viability for resection; however, for many PDAC patients, tumors remain unresectable, even after adjuvant therapy (4).

From the Department of Biomedical Engineering and Mechanics (T.J.O., M.F.L., R.V.D.), Virginia Tech; Virginia Tech-Wake Forest University School of Biomedical Engineering and Sciences (T.J.O., M.F.L., R.V.D.), Blacksburg, Virginia; and Department of Surgery, Division of HPB Surgery (M.P., J.K.S., W.B.L., J.H.S., D.V., E.H.B., D.A.I., I.H.M.), Carolinas Medical Center, 1000 Blythe Boulevard, Charlotte, NC 28203. Received August 23, 2018; final revision received January 23, 2019; accepted January 30, 2019. **Address correspondence to** I.H.M.; E-mail: iain@atriumhealth.org

R.V.D. and M.F.L. have pending and issued patents in the area of irreversible electroporation and may receive royalties. None of the other authors have identified a conflict of interest.

Appendix A, Figures E1–E6, and Tables E1 and E2 can be found by accessing the online version of this article on *www.jvir.org* and clicking on the Supplemental Material tab.

J Vasc Interv Radiol 2019; 30:854–862

https://doi.org/10.1016/j.jvir.2019.01.032

EDITORS' RESEARCH HIGHLIGHTS

- This is a preclinical feasibility study of single-needle high-frequency irreversible electroporation (SN-HFIRE) for pancreatic ablation in an in vivo swine model. Six swine pancreases were treated with open SN-HFIRE without intraprocedural paralytic medications or cardiac synchronization using varying voltage waveform settings (1-5-1, 2-5-2, or 5-5-5 μs, with a total energized time of 100 μs; n = 6 ablations per setting).
- Key measured outcomes included intraprocedural muscle twitch and cardiac activity, as well as ablation zone size and volume 6 hours postprocedure.
- All ablations were technically successful, with no change in muscle twitch or cardiac activity at any pulse setting during the 5-minute ablations. Major findings included larger ablation areas (85 vs. 41/44 mm^2) and volumes (3344 vs. 1162 and 1339 mm^3) using the 5-5-5 μs pulse setting; ablation zone size outcomes were then used to develop lethal electric field thresholds for each pulse setting.
- The results of this small feasibility study support the ability of SN-HFIRE to create rapid ablation zones in pancreatic tissue without intraprocedural paralytic medications or cardiac synchronization. More comprehensive in vivo investigation in larger cohorts and tumor models is necessary.

Thus, a clinical need exists for new approaches to aid surgical margin enhancement and/or ablate tumors in situ.

Irreversible electroporation (IRE) was developed as a nonthermal means of tissue ablation (5,6). The delivery of brief, high-amplitude, pulsed electrical fields between 2 (or more) electrodes increases the transmembrane potential of a cell above a critical threshold and induces permanent membrane poration and irrecoverable disruption of cell homeostasis (7,8). Because IRE induces cell death in the absence of thermal damage to vascular or ductal structures (9), it offers potential advantages compared with thermal ablation in select cases (10,11). The risk of cardiac asynchrony and muscle tetany during IRE means pulse delivery must be synchronized with cardiac activity and is (typically) performed with intraoperative paralytics (12,13). To address these limitations, high-frequency IRE (HFIRE) was developed (14). Unlike IRE (monopolar ≈100 μs pulses), HFIRE uses bipolar square waves of 1–5 μs pulses delivered in a rapid burst, obviating the need for cardiac synchronization and intraoperative paralytics (14,15) (**Fig E1** [available online on the article's Supplemental Material page at *www.jvir.org*]).

Accurately placing multiple electrodes for IRE or HFIRE demands a high level of technical skill (16). Similarly, maintaining electrode position and alignment following placement is critical for ensuring accuracy/completeness of treatment. Previous studies have used single-needle devices for IRE delivery in porcine liver (17,18). The purpose of this study was to determine the efficacy of a single needle, dual-electrode device for HFIRE delivery in an *in vivo* porcine pancreas model and perform numerical modeling techniques using these data to determine the lethal thresholds for HFIRE in pancreas.

MATERIALS AND METHODS

Study Outcome Measurements

The primary outcome measures of this study were to define ablation area and volume in a swine pancreas model for 3 different voltage waveforms (1-5-1, 2-5-2, and 5-5-5 [on-off-on times; μs]). The secondary outcome measures were the effect of SN-HFIRE on muscle twitch and cardiac activity, caspase 3–positive staining as an indicator of apoptosis, and the calculation of lethal thresholds for SN-HFIRE in pancreatic tissue.

Assurances

Female Yorkshire pigs (50–55 kg) were used for these studies (Palmetto Research Swine, Reevesville, South Carolina). All studies were approved by the Institutional Animal Care and Use Committee and conformed to the National Institutes of Health Guide for Animal Care and Use of Laboratory Animals.

Pulse Delivery

A single 18-gauge bipolar electrode (AngioDynamics Inc., Latham, New York; **Fig E2** [available online on the article's Supplemental Material page at *www.jvir.org*]) was used to deliver HFIRE using a custom built HFIRE generator (EPULSUS-FBM1-5, Energy Pulse Systems, Lisbon, Portugal) capable of delivering microsecond, bipolar pulses in rapid bursts. Three bipolar voltage waveforms presenting pulse widths of 1, 2, and 5 μs, with a delay of 5 μs between each change in polarity (1-5-1, 2-5-2, and 5-5-5) were evaluated (**Fig E1** [available online on the article's Supplemental Material page at *www.jvir.org*]). The number of bipolar pulses within each waveform was set to provide an on (energized) time of 100 μs. A total of 300 bursts at a 2250 V amplitude was set per sequence. The delivery parameters chosen were selected based on previous reports demonstrating efficacy with these settings with single needle (19,20) and multineedle HFIRE in liver (14,15). An oscilloscope (DPO2002B, Tektronix Inc., Beaverton, Oregon) was used to monitor the voltage and current waveforms. Input voltage was attenuated using a 1000× high-voltage probe (P5210A, Tektronix Inc.) and current detected via a 10× current probe (2877, Pearson Electronics, Palo Alto, California) (**Fig E3** [available online on the article's Supplemental Material page at *www.jvir.org*]).

Surgical Procedures

Animals were fasted overnight and anesthesia induced (Telazol, 5 mg/kg, intramuscularly; Xylazine, 2 mg/kg, intramuscularly; sodium thiopental, 20 mg/kg, intravenously). Following intubation, anesthesia was maintained with isoflurane by inhalation. Animals were continuously monitored using telemetry and pulse oximetry, and blood

samples (<1 mL) were sequentially drawn for analysis (iSTAT, Abbott, Princeton, New Jersey). A midline incision (15–20 cm) was made, a Balfour retractor placed, and monopolar electrocautery used to divide the gastrocolic ligament to expose the lesser sac. The anterior pancreas surface was visualized, and the tail and distal body mobilized from the spleen. An accelerometer was attached to the abdominal wall adjacent to the intended site of electrode insertion (**Fig 1a**, **Fig E4** [available online on the article's Supplemental Material page at *www.jvir.org*]), and an ultrasound (US) probe used to identify regions distal from major vascular structures (**Fig 1a**).

Before study initiation, a pulse-delivery protocol was designed to ensure each animal received ablations of different waveform settings. The SN-HFIRE device was inserted into the tail of the pancreas and advanced toward the body, or into the pancreatic body and advanced toward the tail (≥3 cm between final placements) and HFIRE delivered. On completion of HFIRE delivery, Doppler mode US was performed to visualize vascular patency (**Fig 1b**). After confirming the absence of bleeding at the site of insertion, the fascia and skin were closed.

Euthanasia and Necropsy

Animals were euthanized (12 mL EUTHASOL) 6 hours after the final ablation. At necropsy, the pancreas was removed, and the ablation sites photographed. The ablation site was sectioned in parallel with and transversely to the plane of electrode insertion, and the ablation region photographed. Pair-matched sections (longitudinal and transverse) were placed in triphenyltetrazolium chloride (TTC) solution (5–10 minutes, 20°C). Following TTC staining, measurements of the transverse and cross-sections were used to calculate the ablation area and volume (15). Tissue samples were then fixed in 10% (v/v) neutral buffered formalin (4°C) overnight.

Histological Analysis and Apoptotic (Caspase 3) Activity

Following fixation samples were prepared and sectioned. Slides stained with hematoxylin and eosin were used to identify the ablation region and examined for signs of thermal damage. To identify necrotic and apoptotic cell death, immunohistochemistry (IHC) was performed on sections using an antibody specific against cleaved caspase 3 (AbCam, Cambridge, Massachusetts) (15). Using scanned IHC images (2 sections/ablation), ImageJ software (NIH, Bethesda, Maryland) was used to measure apoptotic and necrotic regions within the ablation zone. Briefly, the complete ablation zone was selected and the background (nontissue area) subtracted. Threshold techniques were then used to identify cleaved caspase positive (stained brown) and cleaved caspase negative (stained blue) regions. These values were used to calculate the relative area of caspase 3–positive staining present with data expressed as mean percentage cleaved caspase - positive staining ± standard error of the mean.

Numerical Modeling

Finite element models were developed using a finite element package (COMSOL Multiphysics, v.5.4; Stockholm, Sweden) to capture electroporation-induced changes in electrical conductivity, predict electric field distributions, and determine lethal thresholds for SN-HFIRE ablations in pancreatic tissue. The domains consisted of pancreatic tissue modeled as an 84 × 84 × 120-mm ellipsoid with a SN-HFIRE delivery device modeled as cylinders of 8.0 × 1.6 × 7.0 mm (height, diameter, and spacing, respectively) (**Fig E2** [available online on the article's Supplemental Material page at *www.jvir.org*]). Electrical current was measured over a range of voltages during *in vivo* procedures and applied to develop a waveform-specific conductivity curve. Using this curve to differentiate between waveforms within the numerical model, an electric field distribution was predicted, a volume integration performed, and the electric field contours adjusted to match in vivo ablation dimensions and define the lethal threshold for each voltage waveform. Details of the numerical modeling mathematics employed and assumptions are presented in **Appendix A** (available online on the article's Supplemental Material page at *www.jvir.org*) in conjunction with the material properties applied (**Table E1** [available online on the article's Supplemental Material page at *www.jvir.org*]).

Statistical Analysis

In total, 9 animals were used for this study and 2 pancreatic ablations performed per animal (n = 6 ablations for each of the 3 pulse parameters). Sample size was determined based on previous reports using single needle, dual-electrode IRE and multi-electrode HFIRE pulse delivery in other tissue types (15,18,19), from which an *a priori* power analysis was performed (assuming an anticipated effect size [*f*] of 2.5, α of 0.05, and power [1-β] of 0.95, providing a target sample size of 3, which was increased to 6 to account for unanticipated variation between ablations [G*Power 3.1 open source software, Universitat Dusseldorf, Germany]). Data are presented as mean values ± standard error of the mean. Statistical analysis was performed using an ordinary one-way ANOVA with Tukey's multiple comparison using GraphPad Prism software (GraphPad Software, Inc., La Jolla, California). $p < .05$ was considered significant.

RESULTS

Intraoperative and Postoperative Observations

The time taken for SN-HFIRE device placement was <10 minutes, and average pulse delivery time was 5.0 ± 0.2 minutes (n =18). All 9 animals survived the SN-HFIRE procedures for the protocol duration. During HFIRE delivery, no change in cardiac activity or muscle twitch was observed for any of the 3 HFIRE pulse delivery settings used (**Fig E4** [available online on the article's Supplemental Material page at *www.jvir.org*]). Immediately following

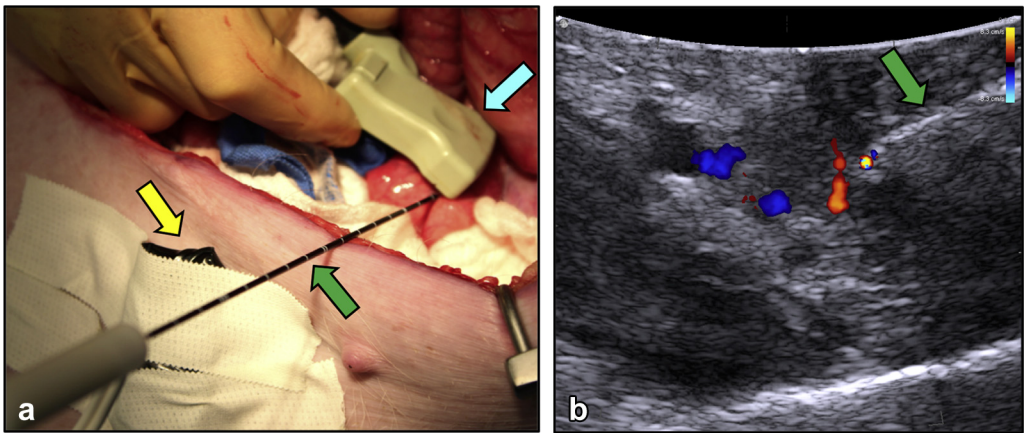

Figure 1. (**a**) Intraoperative image demonstrating pancreatic placement of SN-HFIRE delivery device (green arrow) under US guidance (blue arrow) and placement of accelerometer (yellow arrow). (**b**) Representative Doppler US image captured immediately after completion of SN-HFIRE delivery (green arrow shows the SN-HFIRE delivery device).

Table 1. Physiological Parameters before (Time 0 Hours) and after SN-HFIRE Pancreatic Ablation

Parameter	Time (h)			
	0	2	4	6
Na^+ (mmol)	139.0 ± 0.6	137.0 ± 1.1	136.0 ± 1.4	135.0 ± 1.8*
K^+ (mmol)	4.0 ± 0.4	4.4 ± 0.3	4.8 ± 0.7	5.3 ± 0.9*
Cl^- (mmol)	100.0 ± 1.8	99.0 ± 1.2	98.0 ± 2.4	99.0 ± 1.7
Ca^{2+} (mmol)	1.40 ± 0.09	1.40 ± 0.07	1.40 ± 0.06	1.40 ± 0.08
TCO_2	33.0 ± 2.0	34.0 ± 3.1	33.0 ± 2.2	33.0 ± 2.0
Glucose	117 ± 12	119 ± 10	109 ± 16	97 ± 17
Creatinine (mmol)	1.30 ± 0.17	1.30 ± 0.124	1.60 ± 0.35	2.30 ± 0.46*
Hct	31.0 ± 1.7	30.0 ± 2.2	33.0 ± 2.6	34.0 ± 3.4
Hb2	11.0 ± 0.6	10.0 ± 0.8	11.0 ± 0.9	12.0 ± 1.1

Note–Values are expressed as mean ± standard deviation.
Hb2 = hemoglobin A2; Hct = hematocrit; SN-HFIRE = single-needle high-frequency irreversible electroporation; TCO_2 = total carbon dioxide.
*$p < .05$ versus time 0 hours, n = 6 animals, 2 SN-HFIRE ablations performed per animal.

HFIRE delivery, maintenance of vascular flow at the ablation site was apparent as detected by Doppler mode US (Fig 1b).

Following SN-HFIRE delivery, no significant change in calcium, chloride, total carbon dioxide, hematocrit, or hemoglobin A2 was measured (Table 1). Conversely, potassium and creatinine levels rose significantly, along with a significant decrease in sodium (Table 1). Sequential decreases in blood glucose levels were also observed throughout the study, although these values were not statistically significant (Table 1).

Gross Necropsy and TTC Staining

Gross tissue inspection revealed an overall ellipsoid shaped ablation, the longest ablation axis being parallel to the plane of device insertion (Fig 2a). Following TTC staining, clear demarcation between dead tissue (white-gray) and healthy, metabolically viable tissue (red) was visible (Fig 2b). There was no indication of thermal damage as evidenced by the absence of tissue charring (Fig 2).

Measurement of ablation area revealed no significant differences between pulses delivered at 1-5-1 versus 2-5-2 settings (41.0 ± 5.1 mm^2 vs 44 ± 2.1 mm^2 1-5-1 vs 2-5-2 setting, n = 6 per setting; Table 2, Fig 2c). However, at the 5-5-5 pulse setting, the ablation area was significantly greater than for the other 2 pulse settings used (85.0 ± 7.0 mm^2, $p < 0.0001$ and $p = 0.0001$ versus the 1-5-1 and 2-5-2 settings respectively, n = 6; Fig 2c). Calculation of ablation volume revealed similar differences, with the 5-5-5 setting producing significantly greater ablation volumes than 1-5-1 or 2-5-2 settings, with no significant difference between 1-5-1 and 2-5-2 (3344 ± 403 mm^3 vs 1162 ± 176 mm^3 and 1339 ± 190 mm^3; 5-5-5 vs 1-5-1 and 2-5-2, respectively; $p = 0.0001$, 5-5-5 vs 1-5-1 and $p = 0.0003$ 2-5-2, n = 6 per setting; Table 2, Fig 2c).

Histology and IHC

Histological analysis (hematoxylin and eosin stain) confirmed the area of pancreatic ablation was contained within the region surrounding the SN-HFIRE applicator with clear demarcation between ablated and non-ablated

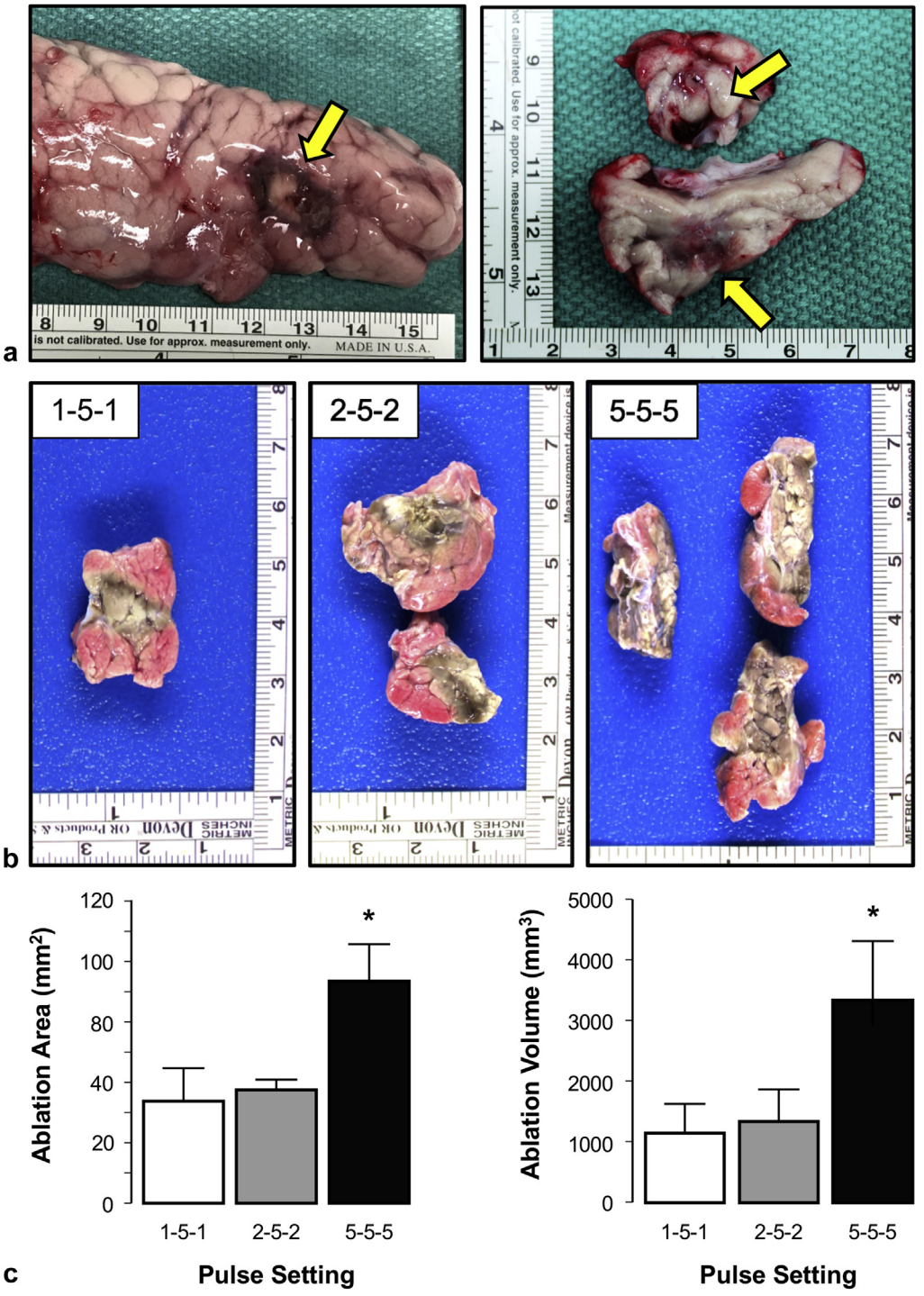

Figure 2. (**a**) Representative image of tail of pancreas at necropsy and after cross-sectioning following SN-HFIRE delivery using 2-5-2 pulse delivery (2250 V). Yellow arrows = ablation site. (**b**) Representative images of pancreatic tissue following TTC staining after SN-HFIRE delivery (2250 V) at 1-5-1, 2-5-2, or 5-5-5 pulse settings. (**c**) Ablation area and volume calculated from measurements taken after TTC staining of pancreatic tissue following SN-HFIRE delivery (2250 V) at 1-5-1, 2-5-2, or 5-5-5 pulse settings. N = 6 per group, Ablation area *$p < .0001$ 5-5-5 vs 1-5-1, $p = .0001$ 5-5-5 vs 2-5-2; ablation volume *$p = .0001$ 5-5-5 vs 1-5-1, $p = .0003$ 5-5-5 vs 2-5-2.

tissue (Fig 3a). Gross structural analysis revealed the apparent preservation of vascular and ductal structures and connective tissue (Fig 3a, Fig E5 [available online on the article's Supplemental Material page at *www.jvir.org*]).

IHC analysis demonstrated cleaved caspase-3 staining was predominantly localized to the margin between healthy and ablated tissue (Fig 3b). Analysis of cleaved caspase 3 staining within the ablation zone demonstrated significantly less cleaved caspase 3–positive staining in cells (vs cleaved caspase 3–negative cells) within the ablation zone for all 3 pulse settings (6.1 ± 2.8% [range 1.8–9.1%), 8.8 ± 1.3% [range 5.5–14.0%), and 11.0 ± 1.4% [range 7.1–14.2%]

Table 2. Ablation Area and Volume Analysis following SN-HFIRE Pancreatic Ablation Area (mm^2)

Pulse Setting	Ablation Area (mm^2)	Range	Median	25th %	75th %
1-5-1	41 ± 5.1	32.1–66.4	37	34	46
2-5-2	44 ± 2.1	38.2–52.0	42	40	49
5-5-5	85 ± 7.0*	63.4–115.4	84	72	95
1-5-1	1162 ± 176	711–1860	1006	843	1592
2-5-2	1339 ± 190	873–2213	1169	1085	1647
5-5-5	3344 ± 403*	2144–4507	3257	2476	4374

Note–Values are expressed as mean ± standard error of the mean.
*$p < 0.05$ 5-5-5 setting versus 1-5-1 and 2-5-2 setting. N = 6 ablations per setting.

cleaved caspase-positive staining; 94.0 ± 2.9% [range 91.0-98.0%], 91.0 ± 3.4% [range 86.0-95.0%], 89.0 ± 3.5% [range 84.0-93.0%] cleaved caspase-negative staining; 1-5-1, 2-5-2, and 5-5-5 settings respectively, n = 6 per group, $p < 0.0001$ cleaved caspase-positive stained versus negative stained cells within treatment groups, **Fig 3c**). In analyzing cleaved caspase 3 staining for the 3 pulse parameters used, the 5-5-5 pulse setting resulted in significantly greater staining than the 1-5-1 pulse setting (6.1 ± 2.8% vs 11.0 ± 1.4%, n = 6 per group, $p = 0.026$).

Numerical Modeling

The parametric sweep analysis yielded a close fit, with R^2 values ≥0.90 for each voltage waveform evaluated (**Table E2** [available online on the article's Supplemental Material page at *www.jvir.org*]). The resulting conductivity curves for each voltage waveform were then plotted (**Fig 4a**). Using these data, the lethal thresholds were determined to be 1114 ± 123 V/cm (1-5-1 waveform), 1039 ± 103 V/cm (2-5-2 waveform), and 693 ± 81 V/cm (5-5-5 waveform) (**Fig 4b**). Finally, 2-dimensional contour plots of the electric field distribution and predicted ablation sizes for each voltage waveform were created (**Fig 4c**).

DISCUSSION

The relative absence of thermal damage and coagulation following IRE (compared with thermal ablation) means the integrity of critical structures within or adjacent to the ablation site remain largely intact. These features offer clinical advantages to IRE for treating tumors with local vascular involvement, including PDAC, which is deemed unsuitable for resection (10,21). Despite these advantages, several clinical and technical challenges associated with IRE remain (21).

In this study, we sought to determine if an SN-HFIRE device could produce rapid, predictable ablations without the need for paralytics or cardiac synchronization within a swine model *in vivo*. The accurate placement and alignment of multiple electrodes for IRE or HFIRE delivery is critical for ensuring intended treatment conditions and avoiding damage to underlying structures, but can be technically challenging (16). For existing IRE therapy, the need for intraoperative paralytics and cardiac synchronization may add difficulty to the procedure; however, the SN-HFIRE approach provides advantages to overcome each of these procedural complications. HFIRE does not require intraoperative paralytics, and no discernable muscle twitch was detected using HFIRE. Similarly, because HFIRE delivery did not cause differences in cardiac function, the need to synchronize pulse delivery with cardiac output is obviated, allowing completion of HFIRE pulse delivery in approximately 5 minutes. Collectively, these data demonstrate the time required to place the SN-HFIRE device (after dissection) and deliver HFIRE was 10–15 minutes. Previous studies have used single-needle devices with IRE pulse delivery in porcine liver (17,18), but none (to our knowledge) have been performed for HFIRE in pancreatic tissue. A major concern associated with single-needle dual electrode IRE devices lies with the potential for limited electric field distribution that result in smaller, thinner ablations (19). From a clinical perspective, this may require multiple overlapping electrode placements to produce the required ablative zone.

At necropsy, there was no visible indication of hemorrhage, and clear demarcation was observed between the ablated and surrounding tissue, observations confirmed by histology and IHC. Of particular note, unlike previous reports using bipolar electrodes for HFIRE delivery in porcine liver (15,22), distribution of cleaved caspase was not uniform within the pancreatic ablation. Rather, the majority of the ablative zone did not stain for cleaved caspase 3, with positive staining being located predominantly at the margin between the ablative zone and healthy tissue. This discrepancy in mechanisms underlying cell death within the ablative field may be due to differences in shear stress placed on cells located within the stronger electrical fields that exist closest to the SN-HFIRE delivery device (8). However, the possibility of thermal damage cannot be discounted, and future studies using fiber optic thermal sensors placed within the ablation zone could be used to determine the effects of HFIRE on tissue heating.

Current measurements across a wide range of voltages throughout HFIRE delivery enabled the development of a voltage waveform-specific numerical model for an SN-HFIRE approach in pancreatic tissue. The model illustrated increased pulse width resulted in an overall tendency for enhanced ablation volume. Lethal thresholds for the SN-HFIRE approach in pancreatic tissue were also established. Further, in agreement with previous studies (23,24), the percentage difference in electrical conductivity (low electric field to high electric field) is inversely related to the pulse frequency. It is anticipated that, as this technology evolves, equivalent

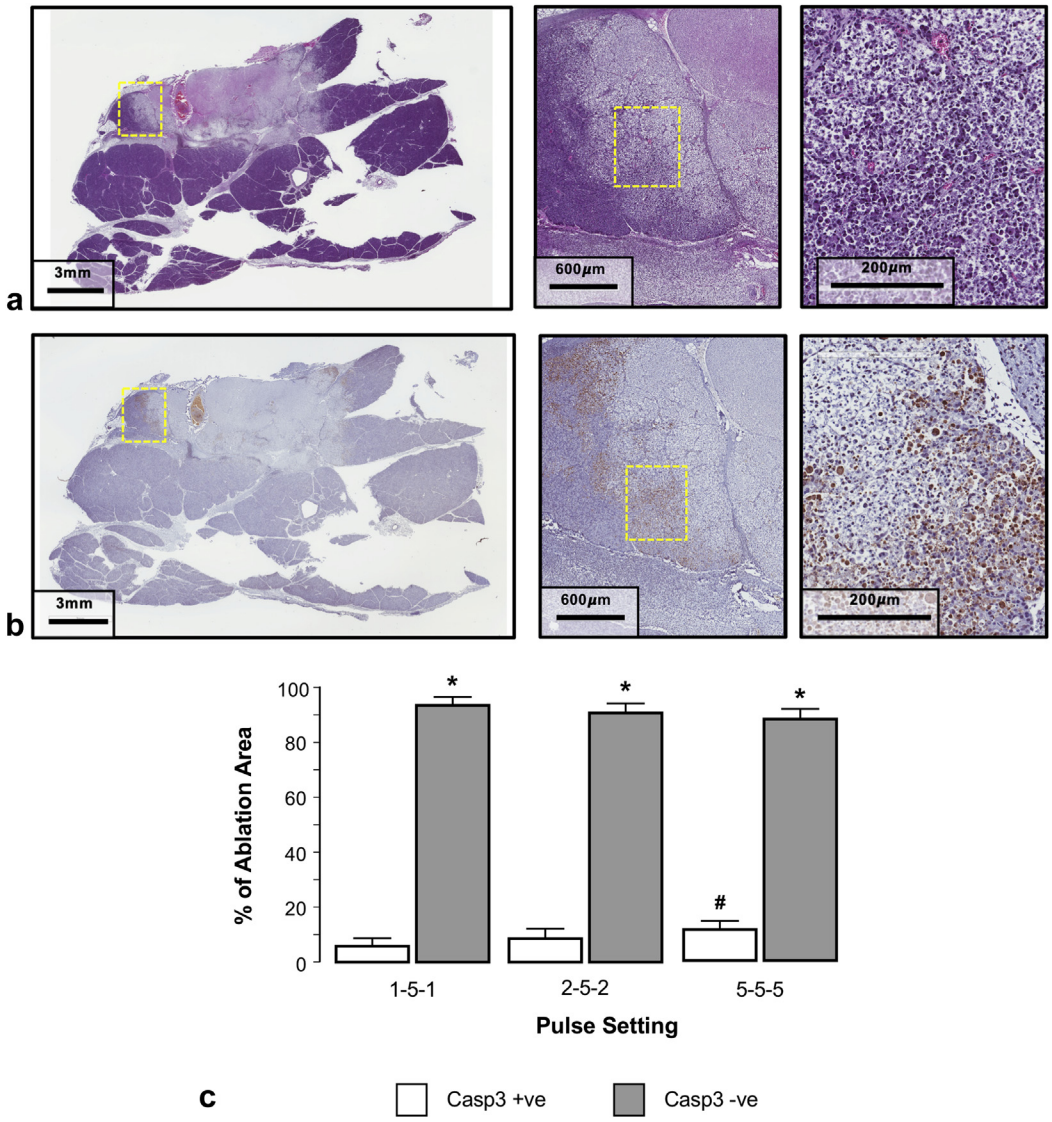

Figure 3. (**a**) Representative hematoxylin and eosin images of pancreatic tissue following SN-HFIRE delivery (2-5-2, 2250 V). The yellow box indicates region of magnification. (**b**) Representative immunohistochemistry images of pancreatic tissue following SN-HFIRE delivery (2-5-2, 2250 V) using an antibody against cleaved caspase 3 (brown stain). Yellow box indicates region of magnification. (**c**) Relative area of cleaved caspase 3 positive (Casp3 +ve) versus cleaved caspase 3 negative (Casp3 –ve) stained tissue. Data are expressed as percentage of total ablation area. N = 6 per group. *$p < 0.0001$ cleaved caspase 3–positive versus cleaved caspase 3–negative staining for each setting. #$p = 0.026$ cleaved caspase 3–positive staining 5-5-5 versus 1-5-1 settings.

models can be created based on these data in which alternative electrode lengths, spacing, or pulse settings are used for pretreatment planning and predicting ablation shape/volume.

Several important study limitations should be considered with the data presented here. From a procedural perspective, it is important to recognize the procedures using SN-HFIRE were performed with an open approach, pancreas dissection was performed before ablation, and the study sample size was designed to use the minimum number of animals based on statistical outcome. In doing so, these conditions do not reflect normal clinical practice for treating PDAC. Future studies have the potential to address these limitations by using a minimally invasive approach (without dissection) and using an expanded sample size with fewer pulse parameters tested. Additionally, within our experimental design, animals were euthanized 6 hours after SN-HFIRE. This protocol was selected because it provides sufficient time to detect and characterize ablations using an IHC-cleaved caspase 3 approach (15,25) to compare *in vivo* ablation characteristics to *in silico* numerical modeling. Based on our data, survival studies may be warranted to follow the apoptotic process to completion, measure pancreas-specific and systemic effects of HFIRE on physiological function, and ascertain the potential impact of HFIRE on tissue immune responses (9,26). In considering the *in silico* modeling performed, it is important to highlight some assumptions made. Specifically, we

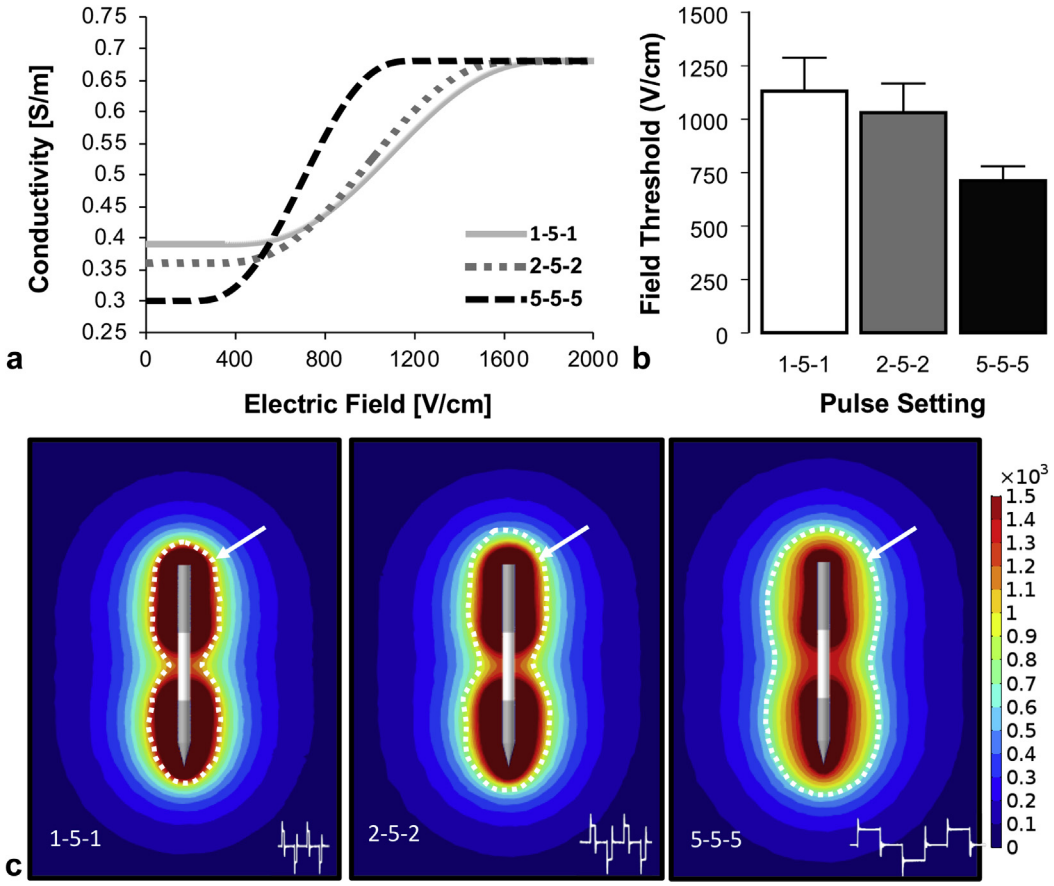

Figure 4. (**a**) Evaluation of dynamic conductivity curves for H-FIRE waveforms for 1-5-1, 2-5-2, and 5-5-5 settings. (**b**) Numerically derived lethal electric field thresholds for 1-5-1, 2-5-2, and 5-5-5 settings waveform settings. (**c**) Two-dimensional contour plot of electric fields for the 1-5-1, 2-5-2, and 5-5-5 H-FIRE waveforms modeled (representative waveform images are in the lower right corner). Calculated lethal thresholds are overlaid as white dotted lines and highlighted (white arrows).

assumed that the end-of-burst voltage and current represent the state of the electric field at all times during HFIRE application, and further represented the electrical conductivity of the tissue without isolation of any tissue capacitive effects, attributing all current contributions to conductive currents. Finally, the data on which ablations were modeled were based on homogenous field distributions in healthy pancreatic tissue, and thus require validation in cancerous tissue. Unfortunately, reproducible large-animal models of PDAC are not readily available. A possible alternative for future studies may be to use resected human PDAC tissue for *ex vivo* analysis of electrical field distribution, or development of a perfused organ system for pancreas similar to those used with liver (15,25).

In conclusion, a single-needle approach for HFIRE delivery can be accurately modeled *in silico* and leads to reproducible pancreatic ablations in a swine model *in vivo*. These data suggest further development of this technology is warranted to optimize electrode arrangements/pulse settings, determine the effects of an SN-HFIRE therapy approach on pancreatic tissue in animal survival models, and measure electrical field distribution in human PDAC tissue *ex vivo*.

ACKNOWLEDGMENTS

The authors thank Dr. W. Carl Jacobs (Board Certified Pathologist, Department of Pathology, MD, 10 years experience) and Dr. Kyle J. Thompson (Instructor, Department of Surgery, PhD, 8 years experience) for their assistance with the analysis of cleaved caspase 3 staining. This work was funded by Pancreatic Cancer Action Network Grant #16-65-IANN.

REFERENCES

1. Ilic M, Ilic I. Epidemiology of pancreatic cancer. World J Gastroenterol 2016; 22:9694–9705.
2. American Cancer Society. Cancer Facts & Figures. Atlanta: American Cancer Society. Available at https://www.cancer.org/content/dam/cancer-org/research/cancer-facts-and-statistics/annual-cancer-facts-and-figures/2018/cancer-facts-and-figures-2018.pdf. Accessed August 1, 2018.
3. Abou-Khalil J, Rocha FG. Surgical strategies and novel therapies for locally advanced pancreatic cancer. J Surg Oncol 2017; 116:16–24.
4. Truty MJ, Thomas RM, Katz MH, et al. Multimodality therapy offers a chance for cure in patients with pancreatic adenocarcinoma deemed unresectable at first operative exploration. J Am Coll Surg 2012; 215:41–52.
5. Lambert L, Horejs J, Krska Z, et al. Treatment of locally advanced pancreatic cancer by percutaneous and intraoperative irreversible electroporation: general hospital cancer center experience. Neoplasma 2016; 63:269–273.

6. Martin RC 2nd, Kwon D, Chalikonda S, et al. Treatment of 200 locally advanced (stage III) pancreatic adenocarcinoma patients with irreversible electroporation: safety and efficacy. Ann Surg 2015; 262: 486–494.
7. Jiang C, Davalos RV, Bischof JC. A review of basic to clinical studies of irreversible electroporation therapy. IEEE Trans Biomed Eng 2015; 62:4–20.
8. Zhang Y, Lyu C, Liu Y, Lv Y, Chang TT, Rubinsky B. Molecular and histological study on the effects of non-thermal irreversible electroporation on the liver. Biochem Biophys Res Commun 2018; 500:665–670.
9. Al-Sakere B, Andre F, Bernat C, et al. Tumor ablation with irreversible electroporation. PLoS One 2007; 2:e1135.
10. Narayanan G, Hosein PJ, Beulaygue IC, et al. Percutaneous image-guided irreversible electroporation for the treatment of unresectable, locally advanced pancreatic adenocarcinoma. J Vasc Interv Radiol 2017; 28:342–348.
11. Al Efishat M, Wolfgang CL, Weiss MJ. Stage III pancreatic cancer and the role of irreversible electroporation. BMJ 2015; 350:h521.
12. Charpentier KP, Wolf F, Noble L, Winn B, Resnick M, Dupuy DE. Irreversible electroporation of the liver and liver hilum in swine. HPB (Oxford) 2011; 13:168–173.
13. Davalos RV, Mir LM, Rubinsky B. Tissue ablation with irreversible electroporation. Ann Biomed Eng 2005; 33:223–231.
14. Arena CB, Sano MB, Rylander MN, Davalos RV. Theoretical considerations of tissue electroporation with high-frequency bipolar pulses. IEEE Trans Biomed Eng 2011; 58:1474–1482.
15. Siddiqui IA, Latouche EL, DeWitt MR, et al. Induction of rapid, reproducible hepatic ablations using next-generation, high frequency irreversible electroporation (H-FIRE) in vivo. HPB (Oxford) 2016; 18: 726–734.
16. Linecker M, Pfammatter T, Kambakamba P, DeOliveira ML. Ablation strategies for locally advanced pancreatic cancer. Dig Surg 2016; 33: 351–359.
17. O'Brien TJ, Bonakdar M, Bhonsle S, et al. Effects of internal electrode cooling on irreversible electroporation using a perfused organ model. Int J Hyperthermia 2018; 35:44–55.
18. Wandel A, Ben-David E, Ulusoy BS, et al. Optimizing irreversible electroporation ablation with a bipolar electrode. J Vasc Interv Radiol 2016; 27: 1441–1450.
19. Sano MB, DeWitt MR, Teeter SD, Xing L. Optimization of a single insertion electrode array for the creation of clinically relevant ablations using high-frequency irreversible electroporation. Comput Biol Med 2018; 95:107–117.
20. Sano MB, Fesmire CC, DeWitt MR, Xing L. Burst and continuous high frequency irreversible electroporation protocols evaluated in a 3D tumor model. Phys Med Biol 2018; 63:135022.
21. Martin RCG 2nd. Multi-disciplinary management of locally advanced pancreatic cancer with irreversible electroporation. J Surg Oncol 2017; 116:35–45.
22. Siddiqui IA, Kirks RC, Latouche EL, et al. High-Frequency Irreversible Electroporation: Safety and Efficacy of Next-Generation Irreversible Electroporation Adjacent to Critical Hepatic Structures. Surg Innov 2017; 24:276–283.
23. Bhonsle SP, Arena CB, Sweeney DC, Davalos RV. Mitigation of impedance changes due to electroporation therapy using bursts of high-frequency bipolar pulses. Biomed Eng Online 2015; 14:S3.
24. Zhao Y, Bhonsle S, Dong S, et al. Characterization of conductivity changes during high-frequency irreversible electroporation for treatment planning. IEEE Transactions on Biomedical Engineering 2018; 65:1810–1819, https://doi.org/10.1109/TBME.2017.2778101.
25. Bhonsle S, Bonakdar M, Neal RE 2nd, et al. Characterization of irreversible electroporation ablation with a validated perfused organ model. J Vasc Interv Radiol 2016; 27:1913–1922.
26. Li X, Xu K, Li W, et al. Immunologic response to tumor ablation with irreversible electroporation. PLoS One 2012; 7:e48749.

APPENDIX A. NUMERICAL MODELING

Assumptions

In numerically modeling the electric field distribution, the following assumptions were made. (*a*) The end-of-burst voltage and current represent the state of the electric field at all times during the application of a high-frequency irreversible electroporation (HFIRE) burst. (*b*) The end-of-burst voltage and current represent the electrical conductivity of the tissue in which any capacitive effects of the tissue were not isolated and all current contributions are attributed to conductive currents. Through experimental application of low- and high-voltage pulses, the changes in tissue conductivity resulting from electroporation are determined. (*c*) The electric field contour pertaining to irreversibly electroporated pancreatic tissue could be determined by matching the experimentally determined volumetric ablation dimensions with those predicted from the numerical model. The electric field that matches these two values was defined as the lethal threshold.

Electric Potential Distribution

The governing equation for the electric potential, Φ at the end of a pulse was determined from equation 1 using the electro-quasistatic approximation and the electric field distribution, $\overline{E}$ by taking the gradient of the electric potential as shown in equation 2:

$$0 = -\nabla\cdot(\sigma\nabla\Phi) \tag{1}$$

$$\overline{E} = -\nabla\Phi \tag{2}$$

where σ is the tissue conductivity. The electrical boundary conditions at the tissue-electrode interface were set to $\Phi = \text{V}$ (source) and $\Phi = 0$ (sink). Boundaries not in contact with an electrode were treated as electrically insulating.

Electrical Conductivity

It is an established phenomenon that high-voltage pulsed electric fields induce changes in electrical properties of biological tissues. These changes are partially attributed to electroporation of the cellular membrane, which creates additional intracellular current pathways, increasing mobility of charged particles (1–3). To account for these changes, a sigmoidal conductivity curve was adapted from (1) using the following equation:

$$\sigma\left(|\overline{E}|\right) = \sigma_0\left(1 + A{\cdot}flc2hs\left(|\overline{E}| - E_{del}, E_{range}\right)\right) \tag{3}$$

Here, σ_0 is the tissue conductivity before electroporation, $|\overline{E}|$ is the magnitude of the electric field vector at any given location, E_{del} is the midpoint of the transition zone, E_{range} determines the span of the transition zone, and A is the multiplier that quantifies the final electroporated state. The *flc2hs* is a smoothed Heaviside function with a continuous second derivative implemented to improve convergence and convergence rate from the sudden transition of conductivity from the unelectroporated state to the electroporated state. In its given form, the function $\sigma(|\overline{E}|)$ changes from σ_0 to $\sigma_0(1 + A)$ over the range $2{\cdot}E_{range}$ with transition starting at $E_{del} - E_{range}$ and ending at $E_{del} + E_{range}$.

A parametric sweep varying σ_0, A, E_{del}, and E_{range} was performed to identify the numerical conditions that best matched the experimental end-of-burst voltage and current for all voltage waveforms (1-5-1, 2-5-2, 5-5-5; Fig E6). An R^2 metric was applied to provide a statistical closeness of fit between the numerically calculated currents and the measured experimental data. Table E2 provides the parameters which yielded the best R^2 results. It should be noted the electrical conductivity at the electroporated state was set to converge to a single value, $\sigma_f = 0.68$ S/m. It has been previously hypothesized that current flow at beta dispersion frequencies tend toward intracellular and extracellular paths. At these frequencies, the capacitive reactance of the cell membrane behaves as a short circuit, channeling current flow through both intracellular and extracellular pathways, similar to that of electroporated tissue (3). The IT'IS database provides conductivity values of 0.603 S/m at a frequency of 1 MHz and 0.794 S/m at a frequency of 100 MHz, providing a lower and upper limit that agrees with the final conductivity determined within this numerical model.

H-FIRE Lethal Thresholds

Following parameter estimation, the waveform-specific electric field distributions were numerically calculated at the end of 300 bursts. To model the effect of multiple pulses on the conductivity distribution, the electric field was computed with the conductivity calculated using equation 4.

$$\begin{aligned}\sigma\left(|\overline{E}|, T\right) =& \sigma_0\left(1 + A{\cdot}flc2hs\left(|\overline{E}| - E_{del}, E_{range}\right)\right)\\ &[1 + \alpha(T - T_0)],\end{aligned} \tag{4}$$

where α is the thermal coefficient of conductivity, T the instantaneous temperature determined from the bioheat equation (detailed below), and T_0 the initial temperature of the tissue (4,5).

Tissue temperature throughout treatment was modeled using a modified Pennes' bioheat equation that incorporates a joule heating term $\sigma|\nabla\Phi|^2$. The modified equation is given in equation 5.

$$\rho c_p\frac{\partial T}{\partial t} = \nabla\cdot(k\nabla T) - \omega_b\rho_b c_b(T - T_b) + \sigma|\nabla\Phi|^2 \tag{5}$$

where ρ is the density of the tissue, c_p is the specific heat of the tissue, k is the thermal conductivity, ω_b is the blood perfusion, ρ_b is the blood density, c_b is the specific heat of the blood, and T_b is the blood temperature. The tissue boundaries were defined as adiabatic at the edge of the domain to illustrate the maximum temperature increase within the tissue model . Further, a duty cycle approach was applied to the thermal simulation, averaging the thermal

energy of a single pulse over a period of 1 second to significantly reduce the computation time. Three hundred bursts of energy were simulated and the final conductivity distribution and electric field distribution were used for the lethal threshold estimations.

The minimum electric field threshold required to induce cell death with H-FIRE (the lethal threshold) was determined by comparing the volumetric ablation dimensions with those produced from the numerical model. The voltage-distance ratios that yielded the best matching dimensions were designated as the lethal thresholds for each voltage waveform. The lethal thresholds for the 1-5-1, 2-5-2, and 5-5-5 were 1113.85 ± 123.2, 1039.47 ± 103.21, and 692.93 ± 80.77 V/cm, respectively.

REFERENCES

1. Zhao Y, Bhonsle S, Dong S, et al. Characterization of conductivity changes during high-frequency irreversible electroporation for treatment planning. IEEE Trans Biomed Eng 2018; 65:1810–1819.
2. Bhonsle S, LorenzoMF, Safaai-Jazi A, Davalos RV. Characterization of nonlinearity and dispersion in tissue impedance during high-frequency electroporation. IEEE Trans Biomed Eng 2018; 65:2190–2201.
3. Neal RE, Garcia PA, Robertson JL, Davalos RV. Experimental characterization and numerical modeling of tissue electrical conductivity during pulsed electric fields for irreversible electroporation treatment planning. IEEE Trans Biomed Eng 2012; 59:1076–1085.
4. Miklavcic D, Sel D, Cukjati D, Batiuskaite D, Slivnik T, Mir LM. Sequential finite element model of tissue electropermeabilisation. Proc IEEE Eng Med Biol Soc 2004; 4:3551–3554.
5. Garcia PA, Rossmeisl JH Jr, Neal RE, Ellis TL, Davalos RV. A parametric study delineating irreversible electroporation from thermal damage based on a minimally invasive intracranial procedure. BioMed Eng OnLine 2011; 34.

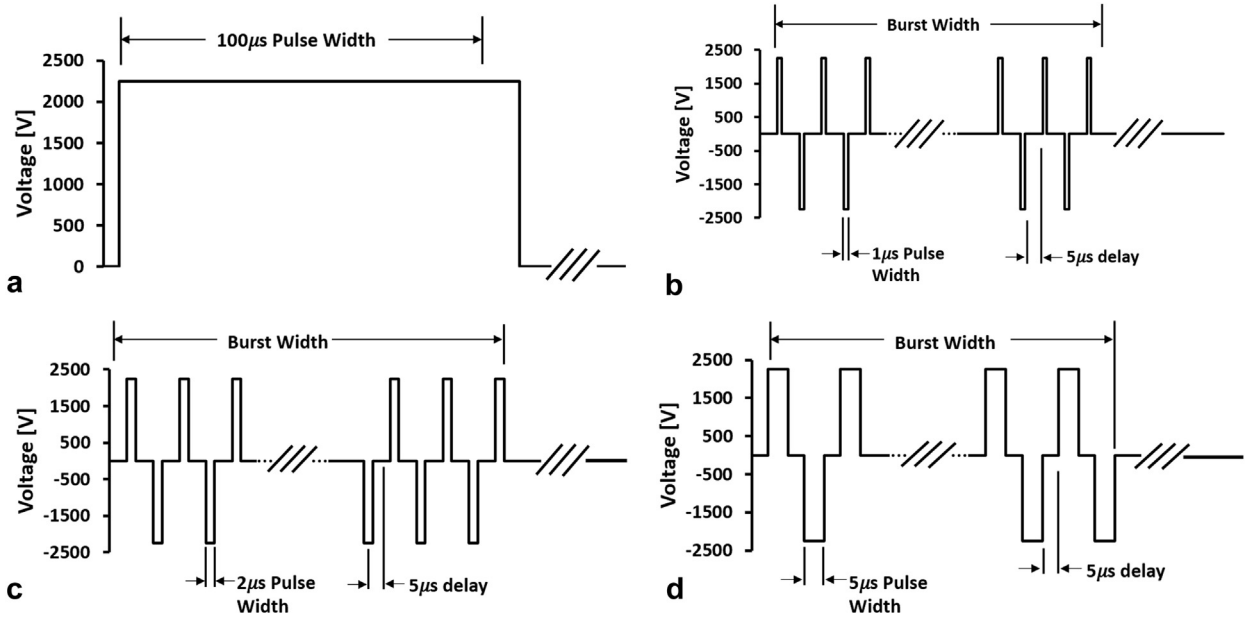

Figure E1. **(a)** Representative image of typical IRE voltage waveform. **(b)** Representative image of 1-5-1 HFIRE voltage waveform. **(c)** Representative image of 2-5-2 HFIRE voltage waveform. **(d)** Representative image of 5-5-5 HFIRE voltage waveform.

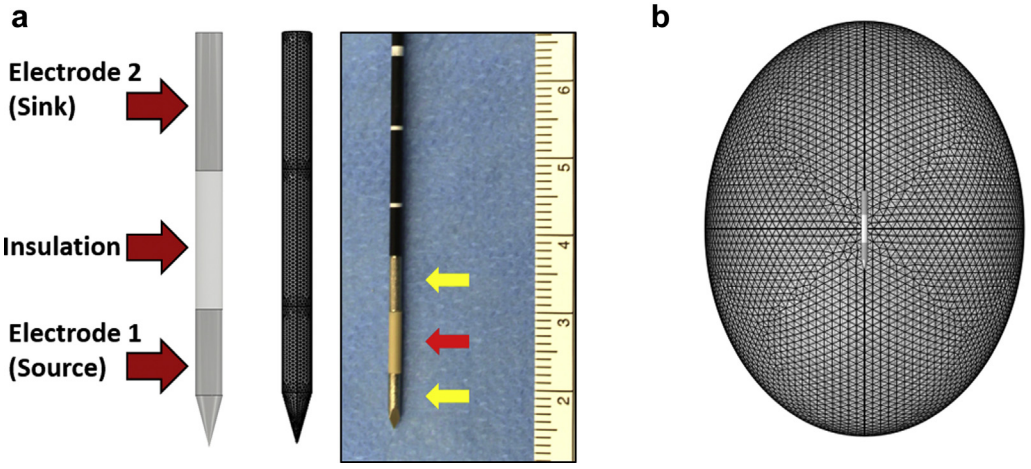

Figure E2. **(a)** Computer rendering of the SN- HFIRE bipolar electrode device alongside image of the SN-HFIRE bipolar electrode device and **(b)** a computer rendering of the device within the pancreatic domain.

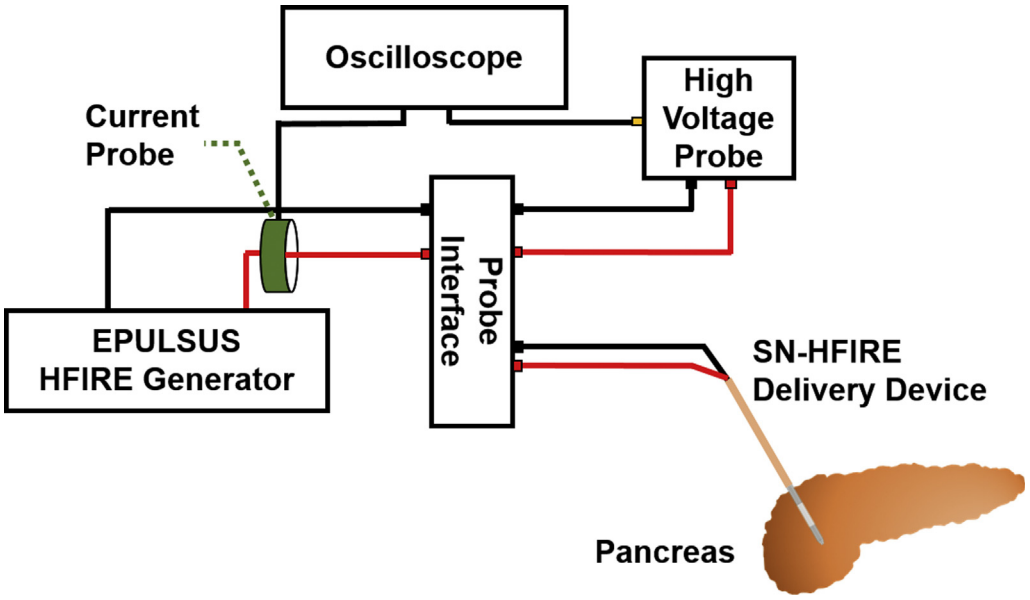

Figure E3. Schematic representation of the equipment setup used for pancreatic SN-HFIRE delivery.

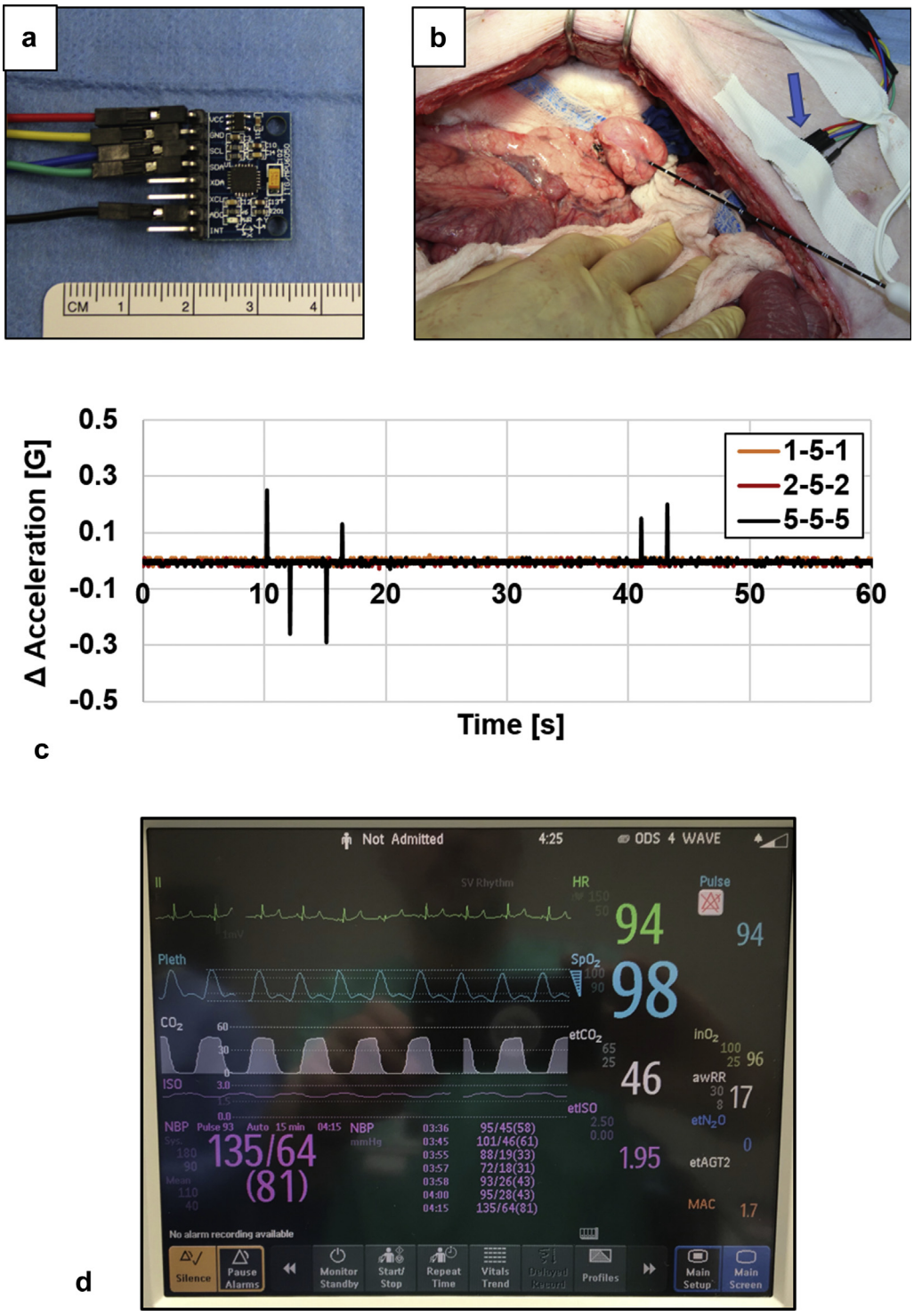

Figure E4. **(a)** Accelerometer used to determine potential muscle movement during SN-HFIRE pulse delivery prior to placement. **(b)** Representative image indicating positioning of accelerometer (blue arrow) during HFIRE delivery. **(c)** Representative accelerometer data for SN-HFIRE delivery for the 1-5-1 (orange line), 2-5-2 (red line), or 5-5-5 (black line) pulse settings employed. **(d)** Representative screen capture of cardiac data obtained during 5-5-5 SN-HFIRE pulse delivery.

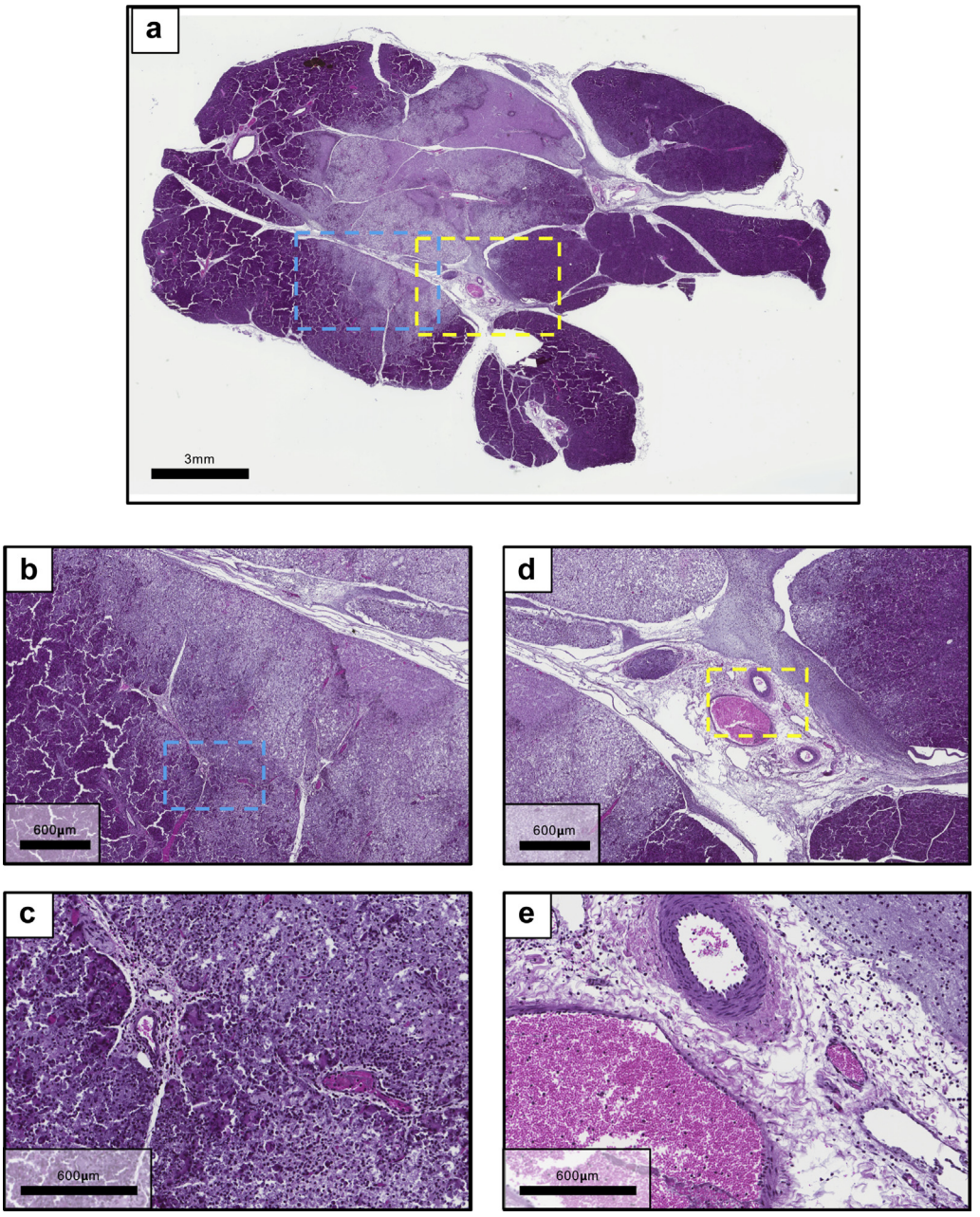

Figure E5. **(a)** Representative H&E image of pancreatic tissue following SN-HFIRE delivery (2-5-2, 2,250V) in which vascular (blue box) **(b, c)** and ductal (yellow box) **(d, e)** are magnified to highlight preservation of architectural integrity at the margins of, and within, the ablative zone.

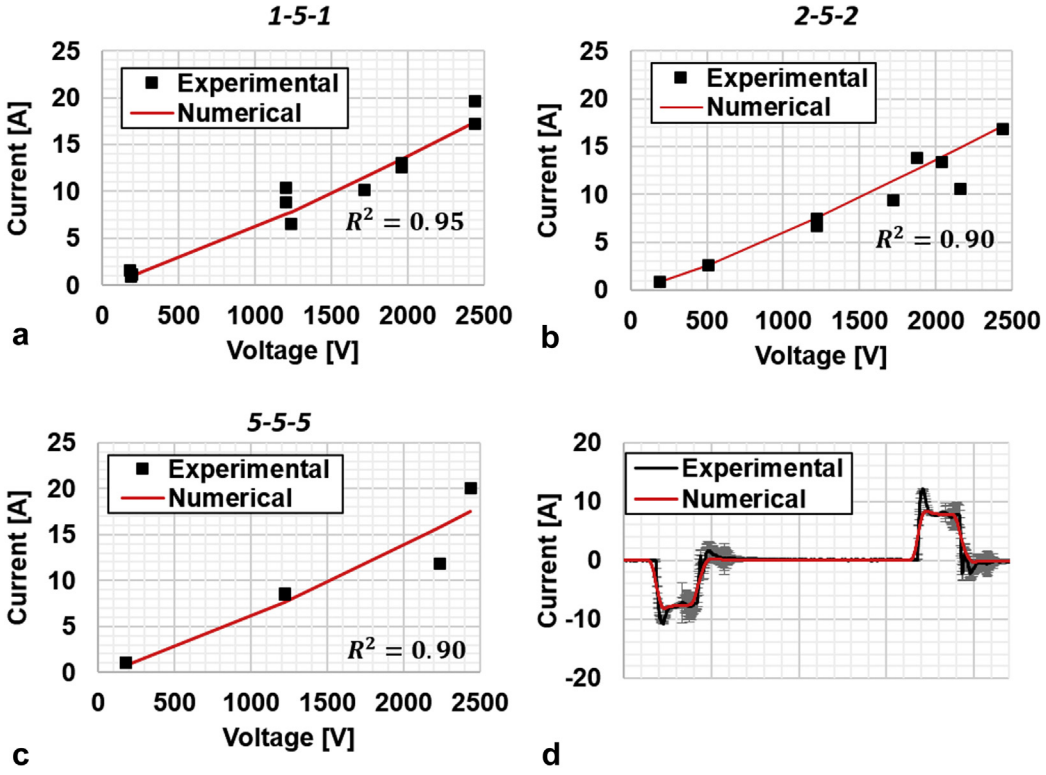

Figure E6. Comparison of experimentally measured and numerically calculated voltage as a function of current for **(a)** the 1-5-1 waveform; **(b)** the 2-5-2 waveform, and **(c)** the 5-5-5 waveform. **(d)** Comparison of the experimental current waveform (n = 3) to the numerically derived current waveform for a 1-5-1 pulse setting. Of note, the experimental data shows an initial sharp peak, representing the capacitive effects of the tissue, which are not capatured within the numerically derived current waveform.

Table E1. Tissue and Probe Properties Used for Numerical Modeling

Material	Parameter	Value	Units
Pancreas	ρ, Density	1087	kg/m^3
	c_p, Heat capacity	3164	$(J/kg)/K$
	k, Thermal conductivity	0.51	$W/(m*K)$
	α, Thermal coefficient of conductivity	0.032	$\%/^{\circ}C$
	ω_b, Perfusion	$7.15e^{-3}$	1/s
Insulation	ρ, Density	2329	kg/m^3
	c_p, Heat capacity	700	$(J/kg)/K$
	k, Thermal conductivity	130	$W/(m*K)$
	σ, Electrical conductivity	$1.0e^{-12}$	S/m
Electrode	ρ, Density	7900	kg/m^3
	c_p, Heat capacity	500	$(J/kg)/K$
	k, Thermal conductivity	15	$W/(m*K)$
	σ, Electrical conductivity	$2.22e^{-6}$	S/m

Note–Data obtained from IT'IS Database for thermal and electromagnetic parameteres of biological tissues, Version 3.0 (Hasgall et al. Available online at www.itis.ethz.ch/database.

Table E2. Parameter Estimation Results for the Numerical Model

Voltage Waveform	σ_0, S/m	A	E_{del}, V/cm	E_{range}, V/cm	R^2
1-5-1	0.39	0.74	1100	750	0.95
2-5-2	0.36	0.89	1000	700	0.90
5-5-5	0.30	1.27	700	500	0.90